

MRI BRAIN CLASSIFICATION USING TEXTURE FEATURES, FUZZY WEIGHTING AND SUPPORT VECTOR MACHINE

**Umer Javed^{1, 3}, Muhammad M. Riaz², Abdul Ghafoor^{2, *},
and Tanveer A. Cheema¹**

¹School of Engineering and Applied Sciences, Isra University, Islamabad, Pakistan

²College of Signals, National University of Sciences and Technology (NUST), Islamabad, Pakistan

³Faculty of Engineering and Technology, International Islamic University, Islamabad, Pakistan

Abstract—A technique for magnetic resonance brain image classification using perceptual texture features, fuzzy weighting and support vector machine is proposed. In contrast to existing literature which generally classifies the magnetic resonance brain images into normal and abnormal classes, classification with in the abnormal brain which is relatively hard and challenging problem is addressed here. Texture features along with invariant moments are extracted and the weights are assigned to each feature to increase classification accuracy. Multi-class support vector machine is used for classification purpose. Results demonstrate that the classification accuracy of the proposed scheme is better than the state of art existing techniques.

1. INTRODUCTION

Magnetic Resonance Imaging (MRI) is a non-invasive imaging technique which provides high contrast images of different anatomical structures. It provides better discrimination of soft tissues than other medical imaging techniques. MRI is frequently being used in detection and the diagnosis of brain tumors [1, 14]. Brain image classification in MRI is an active research area [2, 3–7]. The classification of different

Received 28 May 2013, Accepted 6 July 2013, Scheduled 10 July 2013

* Corresponding author: Abdul Ghafoor (abdulghafoor-mcs@nust.edu.pk).

brain images help in correct treatment. Existing techniques can be broadly classified into supervised [5–7] and unsupervised [9, 10] techniques. Un-supervised techniques do not work in complex scenarios and are based on certain assumptions, such as cluster size etc.. The supervised classification technique work on the principle of training and testing data. These techniques provide better classification accuracy than others [5]. In medical images, noise intensities and textural properties may vary from image to image which may result in poor classification accuracy for supervised methods. These limitations however can be addressed by using invariant features and better classifiers.

Various techniques for classification of images are in literature [2, 11–15]. Gray level thresholding and morphological features based technique does not provide satisfactory results due to complex brain structure and sudden variations in intensities. Segmentation based schemes [11], fail to work if the abnormalities in the brain are not possible to be segmented spatially. Furthermore, the statistical and geometrical variations in brain images limit the performance of these schemes.

Texture analysis based methods often assume that acquired images are already registered which may not always be true. Texture features (by using Gray Level Co-occurrence Matrices (GLCM)) and Artificial Neural Network classify normal and abnormal brain images in [13]. Principal Component Analysis (PCA) and probabilistic neural network based technique uses only spatial signature for brain classification in [12]. In [3], Discrete Wavelet Transform (DWT) based feature extraction, PCA based reduction, adaptive chaotic particle swarm optimization and forward neural network based classification is proposed. The performance of same features are further enhanced using artificial bee colony algorithm in [4] and by using kernel Support Vector Machine (SVM) [5]. The limitations of using PCA with neural networks are discussed in [8]. Schemes based on DWT have limited directionality therefore fails to capture fine details of MRI brain images [7]. Ripplet transform type 1 is used to capture fine details of MRI brain images. A major limitation of above techniques [3–7] is binary classification (only between normal and abnormal brain images). These schemes cannot classify between different abnormal classes because the features (based on DWT and Ripplet transform) are unable to provide separable boundaries. SVM is used in [5] for classifying between normal and abnormal images. In such case, the DWT and PCA technique work well. However, some medical diagnosis systems require to classify between different categories of abnormal images as well [13, 14]. The scheme proposed in [3–7] fails to offer this

kind of classification since the used features have the limited capability of discrimination between abnormal classes.

A fuzzy weighted feature technique is proposed for MRI brain image classification using perceptual texture features, invariant moments, fuzzy weighting and SVM. The proposed technique is designed to classify between normal and different classes of abnormal images. Weights, calculated using fuzzy logic, are assigned to features based on its discrimination capability. Fuzzy logic is used for weight assignment as it provide better performance in case of overlapping boundaries of data [27, 28]. Simulation results show that the proposed technique is able to classify between different abnormal classes and provide better classification accuracy compared to the existing state of art techniques.

2. MRI BRAIN IMAGE CLASSIFICATION

The proposed technique is divided into three steps: feature extraction, weight assignment and classification.

2.1. Feature Extraction

The feature space of the proposed scheme is based on textural features and invariant moments. Textural features can discriminate the texture of different brain diseases while invariant moments provide invariance to rotation and scaling (due to their inherited characteristics) [16]. Textural features (coarseness, contrast, complexity, busyness, shape, directionality, and texture strength) are computed using Neighborhood Gray Tone Difference Matrix (NGTDM) [17].

Let the input X (having dimensions $M \times N$), has total intensities $\{i_1, i_2, \dots, i_C\}$, where i_1 and i_C are the minimum and maximum intensity values, respectively. The NGTDM $t = \{t_1, t_2, \dots, t_C\}$ is defined as,

$$t_c = \sum_{m=1+d}^{M-d} \sum_{n=1+d}^{N-d} \left| i_c - \frac{1}{(2d+1)^2 - 1} \sum_{k_1=m-d}^{m+d} \sum_{k_2=n-d}^{n+d} X_c(k_1, k_2) \right| \quad (1)$$

where d is neighborhood size, X_c the pixel having intensity value i_c , and $c = \{1, 2, \dots, C\}$.

Coarseness measures the degree of intensities local uniformity. The high degree of intensity's local uniformity implies coarse texture. Five different features are then computed from t_c and vice versa. Let

$h = [h_1, h_2, \dots, h_C]$ be the intensity histogram, the coarseness f_1 is,

$$f_1 = \frac{1}{\epsilon + \sum_{c=1}^C h_c t_c} \quad (2)$$

where ϵ is the small constant number for preventing a zero in the denominator and C refers to the highest grey scale level.

Contrast measures the difference between neighboring regions. Low contrast implies that different intensity levels are not clearly visible and vice versa. In MRI images, abnormal tissues may show higher contrast values than normal tissues. The contrast f_2 is,

$$f_2 = \left[\frac{1}{C(C-1)} \sum_{c=1}^C \sum_{b=1}^C h_c h_b (c-b)^2 \right] \left[\frac{1}{(M-2d)(N-2d)} \sum_{c=1}^C t_c \right] \quad (3)$$

Busyness is the measure of sharp intensity changes between two neighbor pixels. Small intensity changes (are not visually noticeable) represent low busyness value and vice versa. Abnormal images have the high spatial frequency of intensity variations. The busyness f_3 is,

$$f_3 = \frac{\left[\sum_{c=1}^C h_c t_c \right]}{\left[\sum_{c=1}^C \sum_{b=1}^C (ch_c - bh_b) \right]} \quad (4)$$

Complexity feature provide visual information of the image. An image with the large number of sharp edges and shapes provide the high complexity value and consequently high degree of information content and vice versa. The complexity f_4 is,

$$f_4 = \sum_{c=1}^C \sum_{b=1}^C \frac{|c-b|}{(M-2d)(N-2d)(h_b+h_c)} (h_c t_c + h_b t_b) \quad (5)$$

Texture strength is also related to the visual perception of the image. If the texture in image is clearly visible and definable then the value of texture strength is high. Texture strength f_5 is,

$$f_5 = \frac{\sum_{c=1}^C \sum_{b=1}^C (c-b)^2 (h_c + h_b)}{\epsilon + \sum_{c=1}^C t_c} \quad (6)$$

The above discussed features can discriminate between different textures of MRI brain images but they are variant to scale, translation and rotation. The textural feature value may change with a slight variance in the input image. To overcome this limitation, these features are combined with invariant moments [16]. These moments, due to their inherited property, are invariant to scale, rotation and translation. The normalized central moments $\eta_{p,q}$ for X are defined as [16],

$$\eta_{p,q} = \frac{\mu_{p,q}}{(\mu_{00})^\zeta} \quad \text{where} \quad \zeta = \frac{p+q}{2} + 1 \quad (7)$$

where $\mu_{p,q}$ is the mean, i.e.,

$$\mu_{p,q} = \sum_{m=0}^{M-1} \sum_{n=0}^{N-1} (m - \bar{m})^p (n - \bar{n})^q X(m, n) \quad (8)$$

and for $p \in \{0, 1, 2, 3\}$ and $q \in \{0, 1, 2, 3\}$

$$\bar{m} = \frac{O_{10}}{O_{00}} \quad \text{and} \quad \bar{n} = \frac{O_{01}}{O_{00}} \quad (9)$$

and

$$O_{pq} = \sum_{m=0}^{M-1} \sum_{n=0}^{N-1} (m)^p (n)^q X(m, n) \quad (10)$$

By the above equations, seven invariant moments can be extracted [16], which are used as feature values, i.e., $\{f_6, f_7, \dots, f_{12}\}$.

2.2. Fuzzy Weight Assignment

As discussed earlier, different weights are assigned to features based on their discrimination capability. Let \hat{i} be the feature class with minimum distance than the difference between individual feature value. The basic idea is to calculate the $\alpha_{\hat{i}}$, the distance between the features of the test image $\tilde{F} = [\tilde{f}_1, \tilde{f}_2, \tilde{f}_3, \dots, \tilde{f}_{12}]$ and the mean feature vector $F^{(i)}$ of each class (normal, sarcoma, meningioma and glioma), i.e.,

$$\alpha_{\hat{i}} = \min_i \|\tilde{F} - F^{(i)}\| \quad (11)$$

where i denotes different classes. The difference between feature value and the mean value is denoted by β_l , \tilde{f}_l denotes test image and f_l^1 represents mean feature value of the first class.

$$\beta_l = |\tilde{f}_l - f_l^1| \quad (12)$$

Previous techniques used to assign all the features of a training set uniform weights. However, in MR image classification, some features

provide better class discrimination over others. In high dimensional image data some feature dimensions appears to be less relevant for classification [18,19]. In this paper, a method for assigning weights based upon its discrimination capability is presented. Instead of binary numbers, real number weights are assigned to all the extracted features.

Let Gaussian Membership Functions (MFs) $\mu_{A^u}(x_1)$ and $\mu_{B^v}(x_2)$ are defined as,

$$\mu_{A^u}(x_1) = e^{-\left(\frac{x_1 - \bar{x}_1^{(u)}}{\sigma_1^{(u)}}\right)^2}, \quad \mu_{B^v}(x_2) = e^{-\left(\frac{x_2 - \bar{x}_2^{(v)}}{\sigma_2^{(v)}}\right)^2} \quad (13)$$

where $u \in \{1, 2, 3\}$ and $v \in \{1, 2, 3\}$, A^1, A^2, A^3 and B^1, B^2, B^3 are input fuzzy MFs corresponds to high, medium and low, respectively. $\bar{x}_1^{(u)}, \bar{x}_2^{(v)}$ and $\sigma_1^{(u)}, \sigma_2^{(v)}$ are constant parameters representing means and variances of fuzzy sets. Gaussian function for mapping the inputs α and β_l into fuzzy domain is,

$$\mu_{AB}(x_1, x_2) = e^{-\left(\frac{x_1 - \alpha}{p_1}\right)^2} \star e^{-\left(\frac{x_2 - \beta_l}{p_2}\right)^2} \quad (14)$$

where \star is the t -norm operator, taken as the algebraic product, and p_1 and p_2 are positive parameters and used for noise suppression in input data, e.g., if p_1 and p_2 are larger than $\sigma_1^{(u)}$ and $\sigma_2^{(v)}$, the noise will be greatly suppressed, so one can choose $p_1 = 2 \max_{u=1}^3 \sigma_1^{(u)}$ and $p_2 = 2 \max_{v=1}^3 \sigma_2^{(v)}$ [27, 28].

Product Inference Engine (PIE) is used to process fuzzy inputs based on fuzzy rule base and linguistic rules [27, 28]. Fuzzy IF-THEN rules for weight assignment are,

- $Ru^{(1)}$: IF α is Low and β_l is Low THEN w_l is Very High.
- $Ru^{(2)}$: IF α is Low and β_l is Medium THEN w_l is High.
- $Ru^{(3)}$: IF α is Low and β_l is High THEN w_l is Medium.
- $Ru^{(4)}$: IF α is Medium and β_l is Low THEN w_l is High.
- $Ru^{(5)}$: IF α is Medium and β_l is Medium THEN w_l is Medium.
- $Ru^{(6)}$: IF α is Medium and β_l is High THEN w_l is Low.
- $Ru^{(7)}$: IF α is High and β_l is Low THEN w_l is Medium.
- $Ru^{(8)}$: IF α is High and β_l is Medium THEN w_l is Low.
- $Ru^{(9)}$: IF α is High and β_l is High THEN w_l is Very Low.

The output MFs are,

$$\mu_{G^r}(y) = e^{-\left(\frac{y - \bar{y}^{(r)}}{\varrho^{(r)}}\right)^2} \tag{15}$$

where $\bar{y}^{(r)}$ and $\varrho^{(r)}$ are constant parameters representing mean and variances of output fuzzy sets. PIE is,

$$\mu_{G'}(y) = \max_{\{r,u,v\}} \left[\sup_{\{x_1,x_2\}} \mu_{AB}(x_1, x_2) \mu_{A^u}(x_1) \mu_{B^v}(x_2) \mu_{G^r}(y) \right] \tag{16}$$

Center average defuzzifier specifies the real output w_l as the weighted sum of 5 output MFs.

$$w_l = \frac{\sum_{r=1}^5 \bar{y}^{(r)} \varpi^{(r)}}{\sum_{r=1}^5 \varpi^{(r)}} \tag{17}$$

where $\varpi^{(r)}$ is the height of μ_{G^r} in r th MF. The transformed feature vector are, $\hat{F} = [\hat{f}_1, \hat{f}_2, \dots, \hat{f}_{12}] = [\tilde{f}_1 w_1, \tilde{f}_2 w_2, \tilde{f}_3 w_3, \dots, \tilde{f}_{12} w_{12}]$.

2.3. SVM Based Classification

SVM is a margin based classifier which achieve superior classification performance compared to other algorithms [21]. The basic principle of SVM is to search for optimal hyperplane with maximal distance of the nearest samples from each class. Let the total images to be classified are K , where $k = 1, 2, \dots, K$, and their respective weighted features are $[\hat{f}_1, \hat{f}_2, \dots, \hat{f}_K]$. The aim is to classify these images into four classes (normal, glioma, sarcoma and meningioma). As discussed earlier, conventional SVM is designed for binary classification. However, multi-class SVM is also in practice. Various techniques have been proposed for modifying binary SVMs to multi-class SVMs. A detailed review of all these algorithms is given in [20, 22].

One-versus-all is the simplest and one of the earliest extensions of SVM for multiclass problems [20, 23]. One-vs-all technique is proven a robust and accurate method for well tuned binary classifiers [23]. In this method, for a K class problem K binary SVM classifiers are required. For i th binary SVM classifier, class i is considered as the positive class whereas the remaining $K - 1$ classes are considered as negative.

Another approach is called the one-versus-one multiclass SVM [22]. Although this approach can effectively decrease the unclassifiable regions that occur in the one-against-all SVMs, the unclassifiable regions still exists. Unlike the one-versus-all multiclass SVM, this method constructs $\frac{K(K-1)}{2}$ binary support vector machines. This scheme determines the class of data by using a voting scheme. The decision function, training procedure and voting mechanism is explained in [20].

Here we have used One-vs-all technique for performing multi-class classification. SVM constructs a binary classifier from a set of labeled pattern called training examples. Let $(\hat{F}_k, g_k) \in \mathfrak{R}^N$, $g^k \in \pm 1, k = 1, \dots, K$ be a set of training examples. The objective is to find a function $f_\alpha : \mathfrak{R}^N \rightarrow \pm 1$ from a given class of functions. SVM maps the nonlinear data to a high dimension space and draws a linear separation surface to separate the training data. Optimal separation surface is achieved by minimizing the margin between vector of classes [24]. Let W represent the feature weight for the training data set,

$$W = \text{diag}(w_1, w_2, \dots, w_{12})^T, \quad 0 \leq w_l \leq 1$$

Therefore, the optimization problem with weighted feature can be written as:

$$\min_{\alpha} : \frac{1}{2} \sum_{j=1}^K \sum_{k=1}^K a_j a_k g_j g_k \Psi(\hat{F}_j W, \hat{F}_k W) - \sum_{j=1}^K \hat{F}_j \quad (18)$$

such that

$$\sum_{k=1}^K a_k y_k = 0, \quad 0 \leq a_k \leq \tau$$

Here ‘ a_k ’ denotes a Lagrange multiplier, ‘ τ ’ controls the misclassification penalty and is a constant. The kernel function is represented by $\Psi(\psi(\hat{F}_j W) \cdot \psi(\hat{F}_k W))$. Global minima can be achieved by presenting the optimization issue in quadratic form [18, 19]. Support vectors help in drawing an optimal hyper-plane. Since SVM’s learning capability relies on the kernel, a Gaussian kernel is used [15, 18].

Classification is done by using decision function once optimal values of all unknown parameters are computed. The final decision function χ becomes,

$$\chi = \text{sgn} \left(\sum_{k=1}^K a_k g_k \Psi(\psi(\hat{F}_j W) \cdot \psi(\hat{F}_k W)) + \vartheta \right) \quad (19)$$

Here ϑ is the bias term. It can be determined from karush-kuhn-tucker condition as in [18]. The outcome of this function decides whether a sample tissue is tumor or non-tumor. The data belonging to $\chi \geq 0$ and $\chi < 0$ is categorized as tumor and non-tumor, respectively. If the feature weights are set to unity, then the above mentioned function will become standard SVM decision function. Hence, the proposed technique is reverse compatible with standard SVM.

2.4. Results and Discussion

The proposed technique is verified using the Harvard medical brain database [25], which consists of MRI T2-weighted images (of 256×256 spatial resolution). The data set contains 48 normal brain images and 25 brain images for each disease. Figures 1(a)–(c) show three different image slices of the normal brain of a same person at the same window size and scanning orientation. Similarly, Figures 1(d)–(f), 1(g)–(i) and 1(j)–(l) are MR image slices belonging to glioma, sarcoma and meningioma classes, respectively. It is important to note that the images of the same class are sometimes quite different (in terms of texture, geometrical and statistical properties) which results in overlapping features. The problem of overlapping features is countered by applying fuzzy weights.

To calculate the texture features using NGTDM [17], three different window sizes (3×3 , 5×5 and 7×7) are used. As the sensitivity of features to spatial changes is dependent upon d [17], therefore average of features over different values of d is evaluated.

NGTDM features (as shown in the Table 1) provide significant differences amongst four classes of MRI brain images. Normal, sarcoma and meningioma effected brain images provide higher values of texture features as compare to the glioma brain images. Normal, sarcoma and meningioma had larger coarseness value than glioma. Normal images show the highest contrast than the tumor effected images whereas meningioma had the lowest contrast. Busyness for normal and sarcoma

Table 1. Mean and variance of texture features for different classes.

Features	Normal	Glioma	Sarcoma	Meningioma
Coarseness	0.8145 ± 0.0040	0.6560 ± 0.0141	0.9231 ± 0.0072	0.7253 ± 0.0121
Contrast	0.9588 ± 0.0004	0.7674 ± 0.0057	0.8861 ± 0.0071	0.6836 ± 0.0015
Busyness	0.9404 ± 0.0035	0.7115 ± 0.0186	0.9004 ± 0.0078	0.6408 ± 0.0148
Complexity	0.9521 ± 0.0003	0.6932 ± 0.0074	0.8759 ± 0.0015	0.6010 ± 0.0043
Strength	0.9712 ± 0.0067	0.7560 ± 0.0046	0.8905 ± 0.0020	0.9196 ± 0.0004

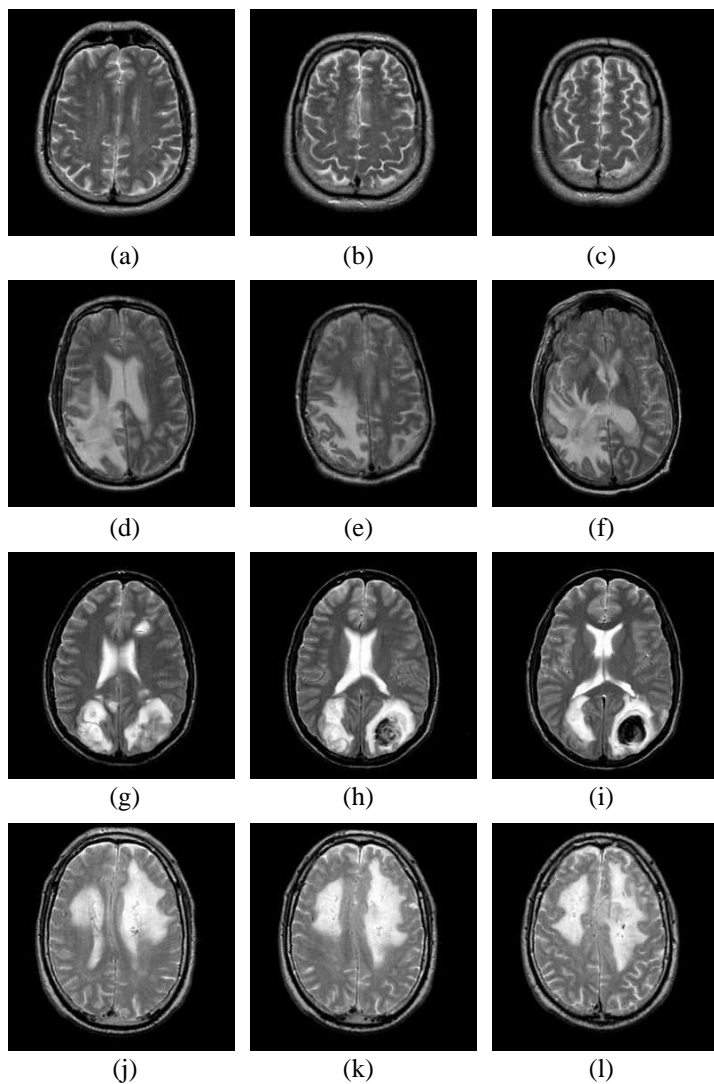


Figure 1. MRI of the human brain. (a)–(c) Normal. (d)–(f) Glioma. (g)–(i) Sarcoma. (j)–(l) Meningioma.

had higher value as compared to rest of classes. Normal and sarcoma images provided higher complexity whereas meningioma had the lowest value. Strength feature for normal images is the highest, but is in similar range for sarcoma and meningioma images.

Table 2 shows the feature values of invariant moments for MR

Table 2. Mean and variance of invariant moments for different orientation.

Features	Degree	Normal	Glioma	Meningioma	Sarcoma
1st moment	0	4.4404 ± 0.0374	3.5473 ± 0.0690	3.4213 ± 0.0395	3.8225 ± 0.0346
	5	4.4033 ± 0.0019	3.5429 ± 0.0789	3.4287 ± 0.0021	3.8334 ± 0.0213
	10	4.4452 ± 0.0056	3.5423 ± 0.0792	3.4279 ± 0.0220	3.8329 ± 0.0211
	15	4.4071 ± 0.0198	3.5427 ± 0.0791	3.4291 ± 0.0022	3.8311 ± 0.0205
	20	4.4101 ± 0.0095	3.4986 ± 0.0975	3.4294 ± 0.0022	3.8333 ± 0.0208
2nd moment	0	0.7202 ± 0.0063	1.2395 ± 0.0034	0.6190 ± 0.0180	1.3178 ± 0.0019
	5	0.7260 ± 0.0018	1.2401 ± 0.0242	0.6171 ± 0.0092	1.3000 ± 0.0506
	10	0.7106 ± 0.0004	1.2406 ± 0.0244	0.6110 ± 0.0097	1.3023 ± 0.0505
	15	0.7155 ± 0.0022	1.2386 ± 0.0254	0.6130 ± 0.0099	1.2981 ± 0.0471
	20	0.7093 ± 0.0002	1.2205 ± 0.0292	0.6144 ± 0.0094	1.3011 ± 0.0502
3rd moment	0	1.7241 ± 0.0414	0.9759 ± 0.1110	0.5412 ± 0.1433	1.4896 ± 0.0227
	5	1.7201 ± 0.0769	0.9820 ± 0.1921	0.5440 ± 0.0401	1.4901 ± 0.0637
	10	1.7175 ± 0.0588	0.9854 ± 0.1879	0.5440 ± 0.0420	1.4860 ± 0.0697
	15	1.7143 ± 0.0872	0.9755 ± 0.1838	0.5457 ± 0.0424	1.4773 ± 0.0667
	20	1.7189 ± 0.0481	0.9642 ± 0.1778	0.5462 ± 0.0406	1.4837 ± 0.0664
4th moment	0	0.0905 ± 0.001	0.3795 ± 0.0077	0.4762 ± 0.0284	0.3646 ± 0.0059
	5	0.0907 ± 0.0103	0.3734 ± 0.0204	0.4701 ± 0.0307	0.3677 ± 0.0377
	10	0.0894 ± 0.0097	0.3743 ± 0.0204	0.4786 ± 0.0306	0.3676 ± 0.0380
	15	0.0929 ± 0.0105	0.3736 ± 0.0205	0.4723 ± 0.0307	0.3686 ± 0.0380
	20	0.0906 ± 0.0102	0.3640 ± 0.0236	0.4798 ± 0.0306	0.3653 ± 0.0364
5th moment	0	0.0316 ± 0.0001	-0.0272 ± 0.0004	-0.1355 ± 0.0165	0.1754 ± 0.0017
	5	0.0293 ± 0.0004	-0.0384 ± 0.0066	-0.1120 ± 0.0017	0.1911 ± 0.0713
	10	0.0332 ± 0.0035	-0.0327 ± 0.0053	-0.2878 ± 0.0549	0.2268 ± 0.0696
	15	0.0364 ± 0.0061	-0.1052 ± 0.0038	-0.2644 ± 0.0292	0.3245 ± 0.0766
	20	0.0324 ± 0.0011	-0.0204 ± 0.0004	-0.2144 ± 0.0257	0.1418 ± 0.0172
6th moment	0	0.0766 ± 0.0022	0.2844 ± 0.0012	-0.2683 ± 0.1722	0.4220 ± 0.0685
	5	0.0766 ± 0.0075	0.2894 ± 0.0145	-0.1921 ± 0.0207	0.4210 ± 0.0713
	10	0.07580 ± 0.0071	0.2899 ± 0.0152	-0.1895 ± 0.0278	0.4250 ± 0.0715
	15	0.0791 ± 0.0078	0.2880 ± 0.0147	-0.1920 ± 0.0278	0.4255 ± 0.0707
	20	0.0763 ± 0.0075	0.2704 ± 0.0180	-0.1917 ± 0.0278	0.4220 ± 0.0685
7th moment	0	-0.0072 ± 0.0000	-0.0232 ± 0.0007	-0.0230 ± 0.0018	-0.2051 ± 0.0001
	5	-0.0028 ± 0.0009	-0.2150 ± 0.0224	-0.0443 ± 0.0090	-0.1450 ± 0.0124
	10	-0.0061 ± 0.0002	-0.0722 ± 0.0006	-0.0765 ± 0.0052	-0.2020 ± 0.0574
	15	-0.0526 ± 0.0058	-0.2521 ± 0.0278	-0.0109 ± 0.0049	-0.2382 ± 0.0812
	20	-0.0145 ± 0.0004	-0.2052 ± 0.0343	-0.0570 ± 0.0099	-0.2085 ± 0.0010

brain images. The first moment had larger value for normal images as compared to the rest. Sarcoma had the highest value for second moment while normal and meningioma had relatively smaller values. Abnormal classes showed much smaller values for third moment than normal class except sarcoma. Fourth moment had the highest value for meningioma while glioma and sarcoma images showed little difference. Sarcoma had higher fifth and sixth moment as compared to all other

Table 3. Mean and variance of invariant moments for different scaling factors.

Moments	Scaling Factor	Normal	Glioma	Meningioma	Sarcoma
1st moment	No scaling	4.4404 ± 0.0374	3.3473 ± 0.0690	3.5213 ± 0.0395	3.6225 ± 0.0346
	0.5	4.0887 ± 0.0114	3.2738 ± 0.0625	3.4298 ± 0.0021	3.8239 ± 0.0172
	0.9	4.3052 ± 0.01732	3.2738 ± 0.0625	3.4300 ± 0.0021	3.8332 ± 0.0021
	1.5	4.3995 ± 0.0012	3.3827 ± 0.0307	3.4324 ± 0.0019	3.8333 ± 0.0209
	2	4.4192 ± 0.0063	3.5354 ± 0.0487	3.4295 ± 0.0021	3.8327 ± 0.0210
2nd moment	No scaling	0.7202 ± 0.0063	0.1805 ± 0.0034	0.7290 ± 0.018	0.1478 ± 0.0019
	0.5	0.6061 ± 0.0008	0.9580 ± 0.0067	0.6140 ± 0.0095	1.2900 ± 0.0004
	0.9	0.6754 ± 0.0013	1.0601 ± 0.0178	0.6150 ± 0.0096	1.3011 ± 0.0041
	1.5	0.7051 ± 0.0004	1.1272 ± 0.0031	0.6452 ± 0.0141	1.3020 ± 0.0490
	2	0.7113 ± 0.0004	1.2334 ± 0.0118	0.6144 ± 0.0094	1.3025 ± 0.0503
3rd moment	No scaling	1.7641 ± 0.0414	0.6459 ± 0.1110	0.3212 ± 0.1433	1.0196 ± 0.0227
	0.5	1.6810 ± 0.0429	0.6641 ± 0.0706	0.5480 ± 0.0041	1.470 ± 0.0610
	0.9	1.6020 ± 0.0618	0.7681 ± 0.1131	0.5461 ± 0.0405	1.4750 ± 0.0670
	1.5	1.7092 ± 0.0635	0.8334 ± 0.0813	0.5534 ± 0.0430	1.4803 ± 0.0639
	2	1.7318 ± 0.0055	0.9642 ± 0.0142	0.5466 ± 0.0407	1.4831 ± 0.0660
4th moment	No scaling	0.0905 ± 0.001	0.1795 ± 0.0077	0.7612 ± 0.2284	0.0746 ± 0.0059
	0.5	0.0714 ± 0.0061	0.2490 ± 0.0058	0.4801 ± 0.0308	0.3622 ± 0.0342
	0.9	0.0844 ± 0.0098	0.2940 ± 0.0133	0.4795 ± 0.0308	0.3658 ± 0.0372
	1.5	0.0892 ± 0.0101	0.3226 ± 0.0134	0.5424 ± 0.0104	0.3663 ± 0.0037
	2	0.0889 ± 0.0009	0.3688 ± 0.0172	0.4792 ± 0.0307	0.3663 ± 0.0372
5th moment	No scaling	0.0316 ± 0.0001	-0.0272 ± 0.0004	0.1355 ± 0.0165	-0.0154 ± 0.0017
	0.5	0.0296 ± 0.0007	0.0232 ± 0.0004	0.0859 ± 0.0049	0.1920 ± 0.0240
	0.9	0.0288 ± 0.0021	0.0341 ± 0.0014	0.0855 ± 0.0047	0.1981 ± 0.0273
	1.5	0.0312 ± 0.0021	0.0451 ± 0.0032	0.1183 ± 0.0054	0.1982 ± 0.0227
	2	0.0308 ± 0.0021	0.0554 ± 0.0039	0.0855 ± 0.0048	0.1990 ± 0.0274
6th moment	No scaling	0.0766 ± 0.0022	0.0144 ± 0.0012	0.6483 ± 0.1722	0.0005 ± 7.00e ⁻⁴
	0.5	0.0559 ± 0.0038	0.1681 ± 0.0028	-0.1911 ± 0.0277	0.4160 ± 0.0626
	0.9	0.0701 ± 0.0017	0.2110 ± 0.0085	-0.1918 ± 0.0021	0.4224 ± 0.0067
	1.5	0.0753 ± 0.0074	0.2400 ± 0.0116	-0.2232 ± 0.0141	0.4232 ± 0.0699
	2	0.0754 ± 0.0027	0.2852 ± 0.0138	-0.1914 ± 0.0002	0.4233 ± 0.0701
7th moment	No scaling	-0.0072 ± 0.0000	0.0232 ± 0.0070	-0.0230 ± 0.0018	-0.0051 ± 0.0001
	0.5	-0.0044 ± 0.0003	0.0427 ± 0.0007	-0.137 ± 0.0081	-0.0792 ± 0.0020
	0.9	-0.0064 ± 0.0001	0.0628 ± 0.0024	-0.1367 ± 0.0081	-0.0812 ± 0.0024
	1.5	-0.0070 ± 0.0001	0.0756 ± 0.0040	-0.1757 ± 0.0051	-0.0819 ± 0.0240
	2	-0.0070 ± 0.0003	0.0719 ± 0.0006	-0.1368 ± 0.0080	-0.0823 ± 0.0024

classes. The seventh moment had the lowest values for sarcoma. Similarly, Table 3 shows invariant moments for different scaling factors (0.5, 0.9, 1.5 and 2).

The performance of our proposed technique is compared with the existing schemes by performing quantitative analysis. A classification system on any occasion can either generate false result to identify an abnormality or it may also classify an abnormality which is not present. The probability that classification test is correctly performed is known

as accuracy. The proposed and existing technique’s accuracy is given for the multi-class problem. The classification results are also tested against different scaling and orientation values.

$$Accuracy = \left(\frac{T_p + T_n}{T_p + T_n + F_p + F_n} \right) \times 100 \tag{20}$$

Here T_p represents True Positive, T_n True Negative, F_p False Positive, and F_n False Negative.

In Figure 2, the classification accuracy of proposed and existing techniques [5, 7] is shown for binary (normal and abnormal) class problem. These techniques are evaluated against different orientation values (Figure 2(a)) and different scaling factors (Figure 2(b)). The results in Figure 2(a), at 0 orientation (reference image), show maximum accuracy but with increase in orientation, the accuracy of Zhang and Wu [5] decreases whereas Das et al. [7] shows relatively stable results. This behavior is due to the limitation of wavelet transform for rotated images [26]. Similar behavior can be observed for different scaling factors in Figure 2(b). The proposed techniques produces less variance in results as the orientation and scale changes. This consistency is due to the fuzzy weights assigned to invariant moments and texture features.

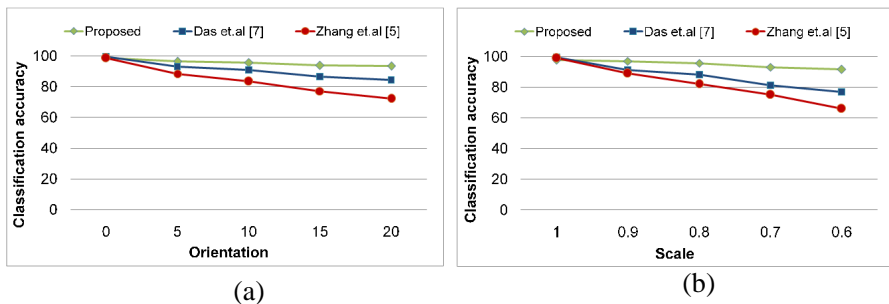


Figure 2. Classification accuracy for binary-class. (a) Against different orientations. (b) Against different scaling factors.

The graphs in Figure 3 show performance evaluation of the existing [5, 7] and the proposed technique for multi-class (normal, glioma, sarcoma and meningioma) classification. Note that the existing techniques provide less accuracy even for zero orientation and unit scale compared to proposed technique. This point out the limitations of early techniques in case of multi-class classification problems. The proposed method provides significantly high classification results for the multi-class problem (normal, glioma, sarcoma and meningioma).

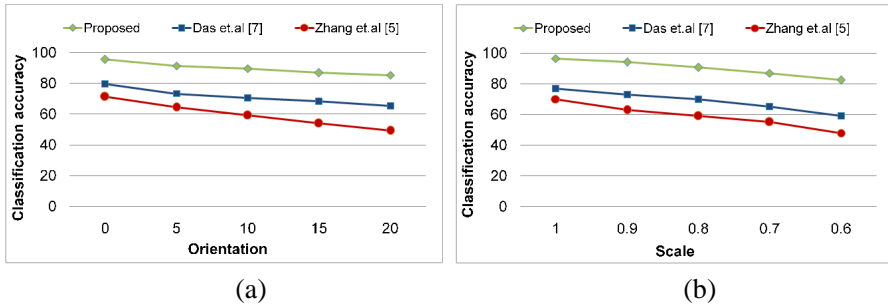


Figure 3. Classification accuracy for multi-class. (a) Against different orientations. (b) Against different scaling factors.

Furthermore, it can be observed from Figure 3 that the proposed technique provides better results at different scales and orientations.

3. CONCLUSION

A technique is proposed for the MRI brain image classification using perceptual texture features, invariant moments and the multi-class SVM. The proposed technique classifies between normal and different classes of abnormal images. Fuzzy logic is used to assign weights to different feature values based on its discrimination capability. The multi class SVM provides better classification accuracy even if the features of different classes have overlapping boundaries. Simulation results show the significance of the proposed technique over state of art existing techniques.

REFERENCES

1. Hakyemez, B., C. Erdogan, N. Bolca, N. Yildirim, G. Gokalp, and M. Parlak, "Evaluation of different cerebral mass lesions by perfusion-weighted MR imaging," *Journal of Magnetic Resonance Imaging*, Vol. 24, No. 4, 817–824, 2006.
2. Lau, P. Y., F. C. T. Voon, and S. Ozawa, "The detection and visualization of brain tumors on T2-weighted MRI images using multiparameter feature blocks," *International Conference of the Engineering in Medicine and Biology Society*, 5104–5107, January 17–18, 2006.
3. Zhang, Y., S. Wang, and L. Wu, "A novel method for magnetic resonance brain image classification based on adaptive chaotic

- PSO,” *Progress In Electromagnetics Research*, Vol. 109, 325–343, 2010.
4. Zhang, Y., L. Wu, and S. Wang, “Magnetic resonance brain image classification by an improved artificial bee colony algorithm,” *Progress In Electromagnetics Research*, Vol. 116, 65–79, 2011.
 5. Zhang, Y. and L. Wu, “An MR brain images classifier via principal component analysis and kernel support vector machine,” *Progress In Electromagnetics Research*, Vol. 130, 369–388, 2012.
 6. El-Dahshan, E.-S., T. Hosny, and A. M. Salem, “Hybrid intelligent techniques for MRI brain images classification,” *Digital Signal Processing*, Vol. 20, No. 2, 433–441, 2010.
 7. Das, S., M. Chowdhury, and M. K. Kundu, “Brain MR image classification using multi-scale geometric analysis of ripplelet,” *Progress In Electromagnetics Research*, Vol. 137, 1–17, 2013.
 8. Malthouse, E. C., “Limitations of nonlinear PCA as performed with generic neural networks,” *IEEE Transactions on Neural Networks*, Vol. 9, No. 1, 165–173, 1998.
 9. Chaplot, S., L. M. Patnaik, and N. R. Jagannathan, “Classification of magnetic resonance brain images using wavelets as input to support vector machine and neural network,” *Biomedical Signal Processing and Control*, Vol. 1, No. 1, 86–92, 2006.
 10. Yeh, J.-Y. and J. C. Fu, “A hierarchical genetic algorithm for segmentation of multi-spectral human-brain MRI,” *Expert Systems with Applications*, Vol. 34, No. 2, 1285–1295, 2008.
 11. Shelvy, P. T., V. Palanisamy, and T. Purusothaman, “Performance analysis of clustering algorithms in brain tumor detection of MR images,” *European Journal of Scientific Research*, Vol. 62, No. 3, 321–330, 2011.
 12. Othman, M. F. and M. A. M. Basri, “Probabilistic neural network for brain tumor classification,” *International Conference on Intelligent Systems, Modelling and Simulation*, 136–138, January 25–27, 2011.
 13. Joshi, D. M., N. K. Rana, and V. M. Misra, “Classification of brain cancer using artificial neural network,” *International Conference on Electronic Computer Technology*, 112–116, May 7–10, 2010.
 14. Zacharaki, E. I., S. Wang, S. Chawla, D. S. Yoo, R. Wolf, E. R. Melhem, and C. Davatzikos, “MRI-based classification of brain tumor type and grade using SVM-RFE,” *IEEE International Symposium on Biomedical Imaging: From Nano to Macro*, 1035–1038, June 28–31, 2009.
 15. Cortes, C. and V. Vapnik, “Support vector networks,” *Machine*

- Learning*, Vol. 20, No. 3, 273–297, 1995.
16. Hu, M. K., “Visual pattern recognition by moment invariants,” *IRE Transactions on Information Theory*, Vol. 8, No. 2, 179–187, 1962.
 17. Amadasun, M. and R. King, “Textural features corresponding to textural properties,” *IEEE Transactions on Systems, Man and Cybernetics*, Vol. 19, No. 5, 1264–1274, 1989.
 18. Vapnik, V., *The Nature of Statistical Learning Theory*, Springer, New York, USA, 1995.
 19. Javed, U., M. M. Riaz, T. A. Cheema, and H. M. F. Zafar, “Detection of lung tumor in CE CT images by using weighted support vector machines,” *International Bhurban Conference on Applied Sciences and Technology*, 113–116, January 15–19, 2013.
 20. Horng, M. H., “Multi-class support vector machine for classification of the ultrasonic images of supraspinatus,” *Expert Systems with Applications*, Vol. 36, No. 4, 8124–8133, 2009.
 21. Anand, A. and P. N. Suganthan, “Multiclass cancer classification by support vector machines with class-wise optimized genes and probability estimates,” *Journal of Theoretical Biology*, Vol. 259, No. 3, 533–540, 2009.
 22. Hsu, C. W. and C. J. Lin, “A comparison of methods for multiclass support vector machines,” *IEEE Transactions on Neural Networks*, Vol. 13, No. 2, 415–425, March 2002.
 23. Rifkin, R. and A. Klautau, “In defense of one-vs-all classification,” *The Journal of Machine Learning Research*, Vol. 5, 101–141, 2004.
 24. Yang, W., H. Xia, B. Xia, L. M. Lui, and X. Huang, “ICA-based feature extraction and automatic classification of AD-related MRI data,” *International Conference on Natural Computation*, 1261–1265, August 10–12, 2010.
 25. Harvard Medical Atlas Database, <http://www.med.harvard.edu/AANLIB/home.html>.
 26. Arivazhagana, S., L. Ganesanb, and T. G. S. Kumara, “Texture classification using ridgelet transform,” *Pattern Recognition Letters*, Vol. 27, No. 16, 1875–1883, 2006.
 27. Riaz, M. M. and A. Ghafoor, “Principle component analysis and fuzzy logic based through wall image enhancement,” *Progress In Electromagnetic Research*, Vol. 127, 461–478, 2012.
 28. Riaz, M. M. and A. Ghafoor, “Spectral and textural weighting using Takagi-Sugeno fuzzy system for through wall image enhancement,” *Progress In Electromagnetic Research B*, Vol. 48, 115–130, 2013.